Int. J. Morphol.,
44(3):789-802, 2026.

http://dx.doi.org/10.4067/s0717-95022026000300789

Investigating the Anticancer Effects of *Ceratonia siliqua* L. (Carob) Bean Extract on Hepatocellular Carcinoma: Insights into Inflammatory, Oxidative Stress, and HOTAIR/miR-124/Notch1 Pathways Using Biochemical, Molecular, Immunohistochemical and Histopathological Methods

Investigación de los Efectos Anticancerígenos del Extracto de Algarrobo *Ceratonia siliqua* L. Sobre el Carcinoma Hepatocelular: Perspectivas Sobre las Vías Inflamatorias, del Estrés Oxidativo y HOTAIR/miR-124/Notch1 Mediante Métodos Bioquímicos, Moleculares, Inmunohistoquímicos e Histopatológicos

Xiaobing Gao[1]; Xiaojun Ying[1]; Dexing Chen[1]; Zhongchao Chen[1]; Xinting Lv[1] & Junbao Wang[1]

GAO, X.; YING, X.; CHEN, D.; CHEN, Z.; LV, X. & WANG, J. Investigating the anticancer effects of *Ceratonia siliqua* L. (Carob) bean extract on hepatocellular carcinoma: insights into inflammatory, oxidative stress, and HOTAIR/miR-124/Notch1 pathways using biochemical, molecular, immunohistochemical, and histopathological methods. *Int. J. Morphol., 44(3)*:789-802, 2026.

SUMMARY: This study evaluated the hepatoprotective and anticancer potential of *Ceratonia siliqua* L. (Carob) bean extract (CSBE) against N-diethylnitrosamine (DEN)-induced hepatocellular carcinoma (HCC) in Wistar rats, focusing on its modulation of biochemical, antioxidant, and molecular pathways, including the HOTAIR/miR-124/Notch1 axis. Fifty rats were divided into five groups: normal controls, DEN-induced HCC (80 mg/kg), HCC treated with 200 or 400 mg/kg CSBE, and normal rats receiving 400 mg/kg CSBE. Post-treatment assessments included serum liver function markers (albumin, total protein, bilirubin, CRP, ALT, AST, ALP), inflammatory cytokines (IL-6, IL-1β, IL-10, TNF-α), oxidative stress parameters (GPx, SOD, CAT, nitric oxide), and molecular analysis of HOTAIR, miR-124, Notch1, and Jagged1 expression in liver tissue, alongside p53 and caspase-3 immunostaining. DEN administration disrupted body/liver weights, elevated liver enzymes, impaired antioxidant defenses, and dysregulated the HOTAIR/miR-124/Notch1 axis, while CSBE—particularly at 400 mg/kg—dose-dependently restored hepatic function, reduced oxidative stress and inflammation, normalized gene expression, and improved histopathological architecture. These findings demonstrate CSBE's efficacy in mitigating DEN-induced HCC through multifaceted mechanisms, highlighting its therapeutic potential.

KEY WORDS: *Ceratonia siliqua* L.; N-diethylnitrosamine; HOTAIR; Liver; Hepatocellular carcinoma.

INTRODUCTION

Hepatocellular carcinoma (HCC), the most common primary liver malignancy, accounts for 500,000–1,000,000 new cases and 600,000 deaths annually, driven by complex molecular mechanisms. Tumorigenesis involves genetic aberrations such as focal deletions in tumor suppressors (PTEN, p53, CDKN2B) and amplifications of oncogenes (MET, MYC, FGF19), coupled with dysregulation of critical signaling pathways including Notch, PI3K/AKT/mTOR, p53/p21, HOTAIR/Notch1, Wnt/β-catenin, and JAK/STAT (Kotsari *et al*., 2023; Wang *et al*., 2024). These alterations disrupt hepatocyte metabolism, cell cycle control, DNA repair, angiogenesis, and immune evasion. Concurrently, pro-inflammatory cytokines (IL-6, IL-1β, IL-10, TNF-α) and oxidative stress mediators (ROS/RNS) synergistically establish a tumor-permissive microenvironment, accelerating malignant transformation (Tabakhiyan *et al*., 2022).

N-nitrosamines, carcinogens formed via nitrous acid and secondary amine interactions, are pervasive in tobacco, processed foods, and environmental pollutants. Among these, N-diethylnitrosamine (DEN) is widely used to model organ-specific carcinogenesis, particularly in the liver. At doses ≥30 mg/kg, DEN induces hepatotoxicity through alkylating metabolites that provoke DNA damage, chronic inflammation, and oxidative imbalance (Janmeda *et al*., 2024). Mechanistically, DEN upregulates G1/S-phase regulators (e.g., cyclin-dependent kinases), while its biotransformation generates ROS/RNS that overwhelm antioxidant defenses, impairing proteins and lipids (Wang *et al*., 2023). This dual action—genotoxic stress and oxidative disruption—makes DEN a robust tool for studying HCC progression and therapeutic interventions. Emerging research highlights the HOTAIR/miR-124/Notch1 axis as a

[1]Department of General Surgery, The First People's Hospital of Yongkang (Yongkang First People's Hospital), No. 599 Jinshan West Road, Yongkang City, Jinhua, Zhejiang Province, 321300, China.

Received: 2025-12-09 Accepted: 2026-02-02

pivotal regulator of liver carcinogenesis. HOTAIR, a long non-coding RNA, epigenetically silences tumor suppressors by recruiting chromatin modifiers, while miR-124, a tumor-suppressive microRNA, inversely modulates oncogenic pathways controlling proliferation and metastasis (Feng *et al*., 2024). Notch1, a transmembrane receptor, and its ligand Jagged1 drive aberrant signaling cascades that sustain tumor growth and chemo resistance (Zhang *et al*., 2021). Dysregulation of this axis correlates with poor prognosis, positioning it as a promising therapeutic target. Investigating natural compounds that modulate this network could unveil novel strategies to counteract HCC progression (Yu *et al*., 2021).

Ceratonia siliqua L. (carob), a Mediterranean evergreen tree cultivated in regions like Spain, Turkey, and China, harbors diverse bioactive compounds. Its bean extract (CSBE) contains polyphenols (catechin, kaempferol), phytosterols, and vitamins with demonstrated antioxidant, anti-inflammatory, and anticancer properties. CSBA's 25–35 % starch content and 10 % pectin contribute to its traditional use in managing diabetes, hyperlipidemia, and gastrointestinal disorders (Dahmani *et al*., 2023; Thomas *et al*., 2024). Preclinical studies reveal its ability to upregulate glutathione-S-transferase (GST), inhibit MMP-2/MMP-9 via TIMP-1/TIMP-2 induction, and induce apoptosis in prostate and gastric cancer cells (Aydemir & Ulusu, 2024). Building on this evidence, our study investigates CSBA's efficacy against DEN-induced HCC in Wistar rats, focusing on its modulation of oxidative stress, inflammatory cytokines, mitochondrial apoptosis, and the HOTAIR/miR-124/Notch1 axis—a multifaceted approach to elucidate its therapeutic potential in liver cancer.

MATERIAL AND METHOD

Preparation of CSBE

Freshly harvested *Ceratonia siliqua* L. beans (3,500 g) were authenticated by a botanist and dried at 35 °C under dark conditions. The dried material was ground into a fine powder using a soil grinder, then mixed with a 70 % ethanol solution (30:30 distilled water-to-ethanol ratio). The mixture was steeped for 72 h at 35°C, after which it was filtered through paper filters and concentrated via rotary evaporation. The final extract (200 g yield) was stored at 4 °C for subsequent use (Ma & Wang, 2025).

Animals and experimental design

Fifty male Wistar rats (220±20 g) were acclimatized for 72 hours under controlled conditions (20±5 °C, 40±10 % humidity, 12/12-hour light/dark cycle) in propylene cages with *ad libitum* access to standard feed and water. Following ethical approval by the First People's Hospital of Yongkang (Yongkang First People's Hospital), the rats were randomized into five groups (n=10): (1) Healthy control (0.5 mL PBS intraperitoneally), (2) HCC model (80 mg/kg DEN in 500 µL PBS intraperitoneally), (3–4) HCC+200 CSBE and HCC+400 CSBE (DEN + 200 or 400 mg/kg oral CSBE), and (5) Healthy+400 CSBE (400 mg/kg oral CSBE alone). Doses were determined via LD50 assessments, preliminary trials, and prior literature, with DEN administered at 9:00 AM and CSBE at 3:00 PM daily. All procedures adhered to institutional guidelines for animal welfare and euthanasia (Table I) (El Sayed *et al*., 2023; Peng *et al*., 2024).

LD50 for CSBE

The LD50 of *Ceratonia siliqua* bean extract (CSBE) was assessed via Lork's two-step method, beginning with nine rats divided into three groups receiving oral doses of 20, 200, and 2,000 mg/kg CSBE, followed by 24-hour monitoring for mortality or toxicity. A subsequent phase involved three additional groups dosed at 100, 500, and 5,000 mg/kg CSBE under identical observation conditions. The LD50 value was calculated using Lork's formula, which integrates the highest non-lethal dose (D safe) and the lowest lethal dose (D toxic) identified during these trials.

$$LD50 = (D\ safe \times D\ toxic)^{1/2}$$ (Zhou *et al*., 2024).

Table I. Animal grouping.

Group number	Group name	Treatment (dose and prescription manner)	Treatment period
1	Control	0.5 ml µl PBS/ i.p.	Day 10, 20 and 30
2	HCC	80 mg/kg DEN dissolved 0.5 ml in PBS/i.p.	Day 10, 20 and 30
3	HCC + 200 CSBE	DEN + 200 mg/kg CSBE / p.o./ p.d.	Day 10 to 40
4	HCC + 400 CSBE	DEN + 400 mg/kg CSBE / p.o./ p.d.	Day 10 to 40
5	Control+ 400 CSBE	400 mg/kg CSBE / p.o./ p.d.	Day 10 to 40

Intraperitoneally injection, p.d.: per day. CSBE: *Ceratonia siliqua* L. bean extract, HCC: hepatocellular carcinoma, DEN: N-diethylnitrosamine, p.o.: per oral, i.p.:

Quantitative analysis of hepatic function and inflammatory markers: serum AST, ALT, ALP, BIL, ALB, TP, and CRP levels

At the study's conclusion, rats were humanely euthanized through a two-step anesthetic process using 50 mg/kg xylazine (2 % solution) and 30 mg/kg ketamine (10 % solution). Cardiac blood samples were collected post-euthanasia, and serum was separated via centrifugation (3,000 rpm for 15 min at 4 °C). Serum concentrations of liver function markers—ALT, AST, AL, BIL, TP, ALB —and the inflammatory marker CRP were measured using standardized ELISA kits (e.g., R&D Systems or Abcam), strictly adhering to manufacturer protocols (Ma *et al*., 2021).

Superoxide dismutase (SOD), catalase (CAT), and glutathione peroxidase (GPx) serum activity

Quantification of antioxidant enzymes (GPx: CSB-E12146r, CAT: CSB-E13439r, SOD: CSB-EL022397RA) in serum was performed using Cusabio's rodent-optimized sandwich ELISA methodology, following standardized operational guidelines (Karimian *et al*., 2025).

Serum nitric oxide (NO) levels

Serum nitric oxide (NO) levels were determined using the Griess colorimetric assay, which measures stable NO metabolites (nitrite and nitrate) given NO's rapid degradation. Serum samples (400 µL) were deproteinized with 6 mg zinc sulfate, centrifuged at 12,000 rpm for 15 min, and 100 µL of supernatant was reacted with 100 µL vanadium chloride (to reduce NO_3- to NO_2-) and Griess reagent containing 1 % sulfanilamide/0.1 % N-(1-naphthyl) ethylenediamine dihydrochloride. After 30-min incubation at 37 °C, absorbance was measured at 450 nm (primary) and 630 nm (reference wavelength for background correction) using a spectrophotometer. NO concentrations were extrapolated from a sodium nitrate standard curve (0–200 µM) and expressed as mmol/L (Li *et al*., 2025).

Liver tissue lipid peroxidation levels (TBARS levels), total antioxidant capacity (FRAP levels), and thiol levels

Liver tissue (100 mg) was homogenized in cold PBS (200 µl) at 4 °C, and 100 µl of the homogenate was mixed with 10 µl of FRAP reagent. The mixture was incubated at 25°C for 15 min, centrifuged at 12,000 × g for 10 min, and the supernatant's absorbance was quantified at 593 nm using a Stat Fax 303 microwell ELISA reader (Awareness Technology, USA).

For thiobarbituric acid-reactive substances (TBARS) analysis, 100 µl of liver tissue homogenate was combined with 100 µl of TBARS reagent, incubated at 37 °C for 30 min, and centrifuged at 12,000 × g for 5 min. Absorbance of the supernatant was measured at 593 nm using the same Stat Fax 303 ELISA reader.

Liver thiol levels were determined by mixing 100 µl of homogenate with 20 µl of 5,5'-dithio-bis-(2-nitrobenzoic acid) (DTNB), incubating at 37 °C for 15 min, and centrifuging at 12,000 × g for 5 min. The supernatant's absorbance was measured at 412 nm (Stat Fax 303 ELISA reader) (Li *et al*., 2025).

Serum levels of IL-1β, TNF-α, IL-10, and IL-6

The anti-inflammatory activity of CSBE was evaluated by measuring serum levels of pro-inflammatory cytokines—TNF-α (Catalog No. NBP2-DY410), IL-6 (Catalog No. M6000B), and IL-1β (Catalog No. RLB00)—along with the anti-inflammatory cytokine IL-10 (Catalog No. R1000), utilizing rodent-specific sandwich ELISA kits (Novus Biologicals, USA) in strict accordance with the manufacturer's protocols (Mi *et al*., 2024).

HOTAIR, miR-124, Notch1, and Jagged1 genes expression

Total RNA was extracted from liver tissue using EX6101-RNX Plus Solution (Cat. No. EX6101-RNX; SinaClon BioScience, China). Tissue homogenization with RNX Plus buffer was followed by chloroform addition (200 µl), phase separation via centrifugation (13,000 × g, 15 min, 4 °C), and isopropanol precipitation (200 ml, ice incubation for 15 min) with subsequent centrifugation (13,000 × g, 15 min). The RNA pellet was washed with 50 % ethanol (1 ml) under identical centrifugation conditions, air-dried, and resuspended in 50 µl nuclease-free water for storage at -80 °C. cDNA synthesis was performed using the Revert AidTM First Strand cDNA Synthesis Kit (Cat. No. K1621; Fermentas, USA) per manufacturer guidelines. Primer sequences for HOTAIR, miR-124, Notch1, Jagged1, and GAPDH (reference gene) were designed with Gene Runner software (Hastings Software, USA) and validated via NCBI Primer-BLAST (Table II). Amplification involved 42 cycles (Corbett Rotor thermocycler) with 70 °C annealing, and gene expression was quantified using ΔΔCt analysis with fold-change calculations relative to GAPDH.

The fold formula change = $2^{-\Delta\Delta CT}$; ΔΔCt = [(Ct sample - Ct GAPDH gene) - (Ct sample – Ct control)] (Li *et al*., 2025).

Table II. Primer sequences.

Gene	Sequences (5'–3')
GAPDH	F: TGAAGGTCGGAGTCAACGG R: AGAGTTAAAAGCAGCCCTGGTG
HOTAIR	F: GGTAGAAAAAGCAACCACGAAGC R: ACATAAACCTCTGTCTGTGAGTGCC
Jagged1	F: CGCCCTCTGAAAAACAGAAC R: ACCCAAGCCACTGTTAAGACA
Notch1	F: CTGGACCCCATGGACATC R: ACTGTACACACTGCCGGTTG
miR-124	F: GGAACCTTCTGAGTGCCTTAC R: CCGTAAGTGGCGCACGGAAT

Immunohistochemistry (IHC) assay

Apoptotic differentiation in liver tumor cells was assessed via p53 and caspase-3 immunohistochemistry. Paraffin-embedded liver tissue sections (5 µm) were deparaffinized, rehydrated, and subjected to heat-induced antigen retrieval by overnight incubation at 95 °C in a Cole-Parmer WB-400 water bath incubator (Model UX-12105-90; Cole-Parmer, USA) with anti-p53 (1:500 dilution; Cat. No. GAF1355) and anti- caspase-3 (1:500 dilution; Cat. No. MAB835) primary antibodies (R&D Systems, USA). Slides were then incubated for 1 h at 25 °C, washed with 0.1 % PBST, and blocked with 5 % bovine serum albumin. Endogenous peroxidase activity was quenched with 3 % H_2O_2 (20 min, 25 °C), followed by DAB chromogen staining and hematoxylin counterstaining. Slides were imaged at 400× magnification using an Olympus BX61TRF microscope (Japan) coupled to ImageJ software. The percentage of p53 and caspase-3-positive cells was calculated by counting positive nuclei across 10 random fields relative to total cells (Khorshed *et al*., 2025).

Liver histopathology

Liver tissues were fixed in 10 % neutral buffered formalin for 72 h, followed by PBS rinsing to remove excess fixative. Specimens underwent sequential dehydration through a graded ethanol series (70 %-100 %), cleared in xylene, and embedded in paraffin wax. Tissue sections (5 µm thickness) were cut using a Leica SM2010RV1.2 microtome (Germany) and heat-adhered to slides at 37 °C. After H&E staining using standard protocols, histological evaluation was performed at 400× magnification with an Olympus BX61TRF microscope (Japan). Digital images were acquired through the integrated camera system and analyzed using ImageJ software (NIH) for quantitative assessment (Naseri *et al*., 2019).

Tissue preparation and stereological measurements

Initial tissue volume was determined using Cavalieri's Principle to account for shrinkage artifacts. The primary liver volume was measured via water displacement in a graduated beaker, with the displacement difference representing the pre-fixation volume. To ensure unbiased sampling, isotropic uniformly random (IUR) sections were generated using the Orientator method: tissues were sequentially bisected along two orthogonal planes defined by randomized angles (0–10° increments), followed by systematic sectioning into 2 mm slices. Six to eight representative sections per liver were selected, and a circular subsample (diameter measured with calipers) was processed through graded ethanol dehydration, xylene clearing, and paraffin embedding at 55 °C. Tissue shrinkage was quantified by measuring the post-processing diameter of circular sections and applying the formula:

$$\text{Volume shrinkage} = 1 - (AA/AB)1.5$$

On 5-µm thickness sections, the volume density of the targeted structures [volume (mm^3) of the totlal (TV) central (HA) and portal veins (PV), bile ducts (BD), and hepatic artery (HA)] was determined using the point-counting method and Delesse's-formula.

$$Vv(structure) = \sum_{i=1}^{n} p\,(structure) / \sum_{i=1}^{n} (reference)$$

"$\sum_{i=1}^{n} p\,(structure)$" was the number of test points that settled on the targeted structures, and "$\sum_{i=1}^{n} p$ " was the total number of points that fell on the liver sections. The following formula was used to determine the total targeted structural volume (Fig. 1).

$$V\,(\text{structure}) = V\,(\text{total liver}) \times Vv\,(\text{structure}).$$

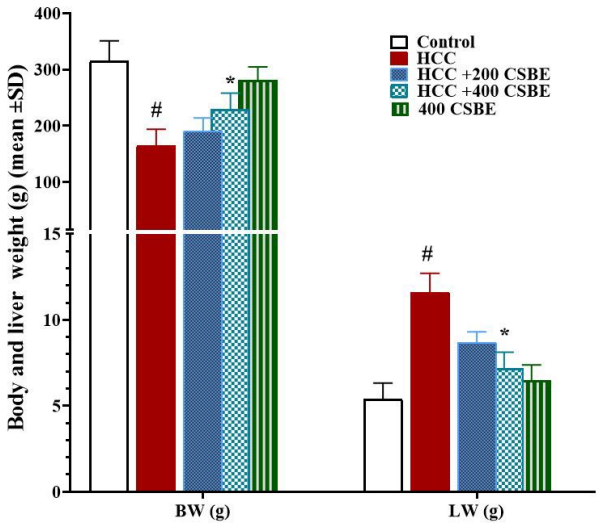

Fig. 1. (a) Rats body (BW) and liver (LW) (g) weight in experimental groups (means ± SD; n=10/group). # ($p<0.05$) HCC *vs*. control groups; * ($p<0.05$) HCC+200 and 400 CSBE treated *vs.* HCC groups.

Statistical Analysis

Quantitative comparisons across experimental groups were performed using one-way analysis of variance (ANOVA) with Newman-Keuls post hoc testing, where statistical significance was defined as $p < 0.05$. Data normality and homogeneity of variances were verified via the Kolmogorov-Smirnov test, with $p > 0.05$ confirming parametric assumptions. Results are expressed as mean ± standard deviation (SD). All analyses were executed in SPSS (v16; IBM Inc., USA), while graphical visualizations were generated using GraphPad Prism (v9; GraphPad Inc., USA) (Naseri *et al*., 2019).

RESULTS

LD_{50} of CSBE

Following a 24-hour evaluation of CSBE-treated groups, a non-toxic safety threshold (D safe) was identified at 2000 mg/kg, while the toxicological limit (D_{toxic}) was observed at 5000 mg/kg. Application of Lorke's method yielded a median lethal dose (LD_{50}) of 3162 mg/kg for CSBE, indicating that doses below this threshold are pharmacologically viable for preclinical animal studies. Normative safety protocols were confirmed through these parameters, ensuring experimental integrity in subsequent toxicological assessments.

Body and liver weight

Upon examining the effects on total body weight (BW) and liver weight (LW), it was found that DEN in the HCC group resulted in a significant decrease in BW ($p < 0.05$) and a notable increase in LW ($p < 0.05$) compared to the healthy group. Conversely, CSBE demonstrated a dose-dependent effect at doses of 200 and 400 mg/kg in the HCC+200 and HCC+400 groups, leading to a significant increase in the rats' weight ($p < 0.05$) and a significant reduction in liver weight compared to the HCC group (Fig. 1).

Effects of CSBE and DEN on serum liver biochemical parameters

Following the evaluation of serum liver enzyme activities (ALT, AST, and ALP), it was found that DEN significantly increased ($p < 0.05$) the activity levels of all three enzymes compared to the control group. In contrast, the HCC+200 and HCC+400 mg/kg CSBE treatment groups demonstrated a significant reduction ($p < 0.05$) in the activity levels of these enzymes when compared to the HCC group. Additionally, the analysis of serum bilirubin (BIL) and C-reactive protein (CRP) levels revealed a significant increase ($p < 0.05$) in both markers within the HCC group relative to the control group. Notably, CSBE showed a dose-dependent effect in lowering ($p < 0.05$) these serum indicators compared to the HCC group. Furthermore, the assessment of serum albumin (ALB) and total protein (TP) levels indicated that DEN significantly decreased ($p < 0.05$) both markers compared to the control group, while the HCC+400 mg/kg CSBE treatment group exhibited a significant increase ($p < 0.05$) in these levels compared to the HCC group (Fig. 2a,b).

Serum GPx, CAT, and SOD activity alongside serum NO levels

DEN induced a significant increase in serum nitric oxide (NO) levels compared to the control group by promoting the generation of free radicals. In contrast, CSBE demonstrated a dose-dependent decrease in NO levels relative to the HCC group, with a statistically significant reduction ($p < 0.05$) observed at the 400 mg/kg dosage in the HCC+400 CSBE group. Additionally, DEN significantly reduced the serum activity of all three antioxidant enzymes compared to the control group. Conversely, CSBE increased the serum levels of these enzymes in a dose-dependent manner, with a statistically significant rise ($p < 0.05$) noted at the 400 mg/kg dosage in the HCC+400 CSBE group compared to the HCC group (Fig. 2c).

Thiol, FRAP, and TBARS levels in liver

Thiol, FRAP, and TBARS levels were important indicators of overall antioxidant capacity and lipid peroxidation. The results showed that DEN significantly reduced ($p < 0.05$) the levels of all three markers in the tissues compared to the control group. In contrast, CSBE, due to its rich antioxidant properties, exhibited a dose-dependent increase in the levels of these markers when compared to the HCC group, with a statistically significant elevation ($p < 0.05$) observed at the 400 mg/kg dosage in the HCC+400 CSBE group compared to the HCC group (Fig. 2d).

Serum levels of TNF-α, IL-10, IL-6, and IL-1β

DEN promoted inflammatory responses, resulting in increased concentrations of pro-inflammatory cytokines and a decrease in systemic anti-inflammatory cytokines. Specifically, there was a significant rise ($p < 0.05$) in the serum levels of all three pro-inflammatory cytokines: TNF-α, IL-1β, and IL-6, compared to the control group, while IL-10 levels decreased notably. Conversely, the study

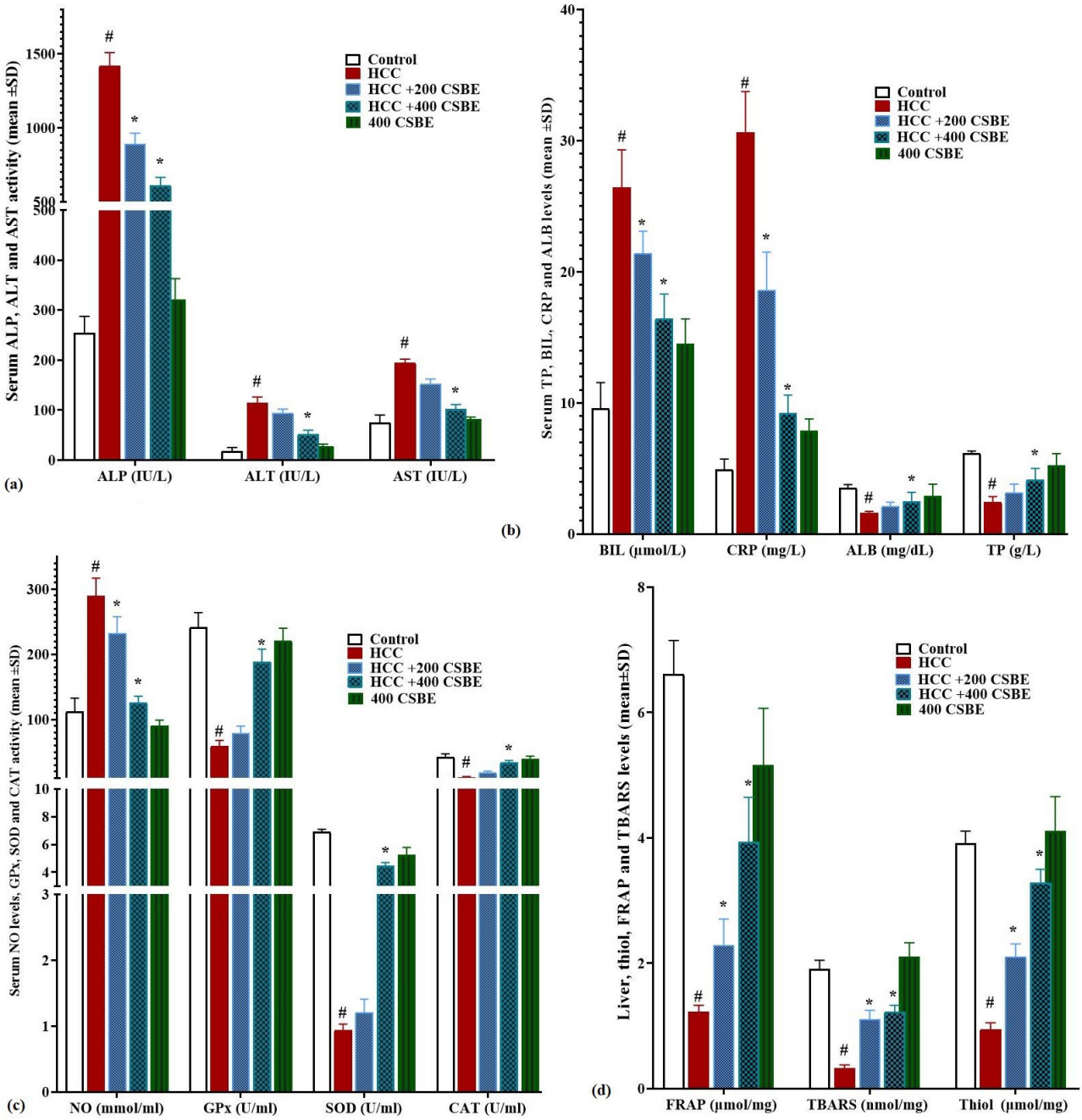

Fig. 2. (a) Serum activity of alanine aminotransferase (ALT), aspartate aminotransferase (AST), and alkaline phosphatase (ALP) enzymes (IU/L), (b) serum levels of albumin (ALB) (mg/dL), total protein (TP) (g/L), and bilirubin (BIL) (µmol/L), C reactive protein (CRP) (mg/L), (c) Serum levels of NO (mmol/ml), alongside the mean serum activity of SOD, CAT, and GPx (U/ml), and (d) liver tissue levels of TBARS (nmol/mg) and FRAP (µmol/mg) in experimental groups (means ± SD; n=10/ group) in experimental groups. # ($p<0.05$) HCC *vs.* control groups; * ($p<0.05$) HCC+200 and 400 CSBE treated *vs.* HCC groups.

indicated that CSBE exhibits strong anti-inflammatory properties, as it progressively increased serum levels of IL-10 and reduced the levels of TNF-α, IL-1β, and IL-6 when compared to the HCC group. These changes were statistically significant ($p < 0.05$) at the 400 mg/kg dosage in the HCC+400 CSBE group compared to the control group (Fig. 3a).

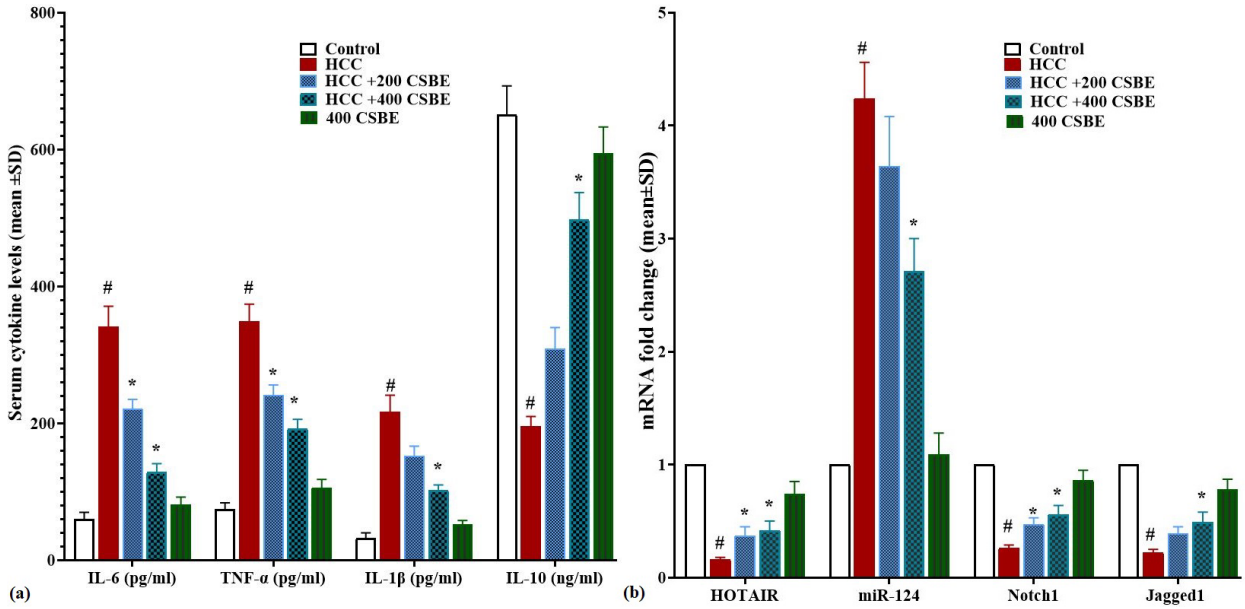

Fig. 3. (a) Serum levels of IL-1b, TNF-a, IL-6 (pg/ml), and IL-10 (ng/ml) and (b) HOTAIR, miR-124, Notch1, and Jagged1 genes expression (means ± SD; n=10/group) in experimental groups. # ($p<0.05$) HCC *vs.* control groups; * ($p<0.05$) HCC+200 and 400 CSBE treated *vs.* HCC groups.

Expression of liver HOTAIR, miR-124, Notch1, and Jagged1 genes

The analysis of gene expression related to proliferation, differentiation, and apoptosis pathways showed that DEN treatment significantly decreased the expression of HOTAIR, Notch1, and Jagged1, while increasing miR-124 expression in hepatocytes compared to the healthy group ($p < 0.05$). In the HCC+200 CSBE group, there was an increase in HOTAIR, Notch1, and Jagged1 expression, along with a decrease in miR-124 expression compared to the HCC group; however, these changes were not statistically significant ($p > 0.05$). The most notable changes occurred in the HCC+400 CSBE group, where HOTAIR, Notch1, and Jagged1 expression significantly increased, and miR-124 expression significantly decreased compared to the HCC group ($p < 0.05$). (Fig. 3b).

Liver tissue stereology parameters

Liver volume assessment showed that DEN exposure caused a significant increase ($p < 0.05$) compared with the control group, based on measurements of hepatocyte and sinusoid volumes. Among the CSBE-treated groups, only the 400 mg/kg dose produced a significant reduction in liver volume relative to the DEN group. Analysis of the central vein, portal vein, bile duct, and hepatic artery volumes revealed that the DEN group exhibited significantly larger central and portal veins and a markedly reduced bile duct volume compared with the control group ($p < 0.05$), while hepatic artery volume remained unchanged ($p > 0.05$).

Treatment with 400 mg/kg CSBE significantly increased the volumes of the central and portal veins and significantly decreased bile duct volume ($p < 0.05$). In contrast, the 200 mg/kg CSBE group showed no statistically significant differences ($p > 0.05$), although the measured volumes tended to return toward normal levels (Figs. 4 and 5).

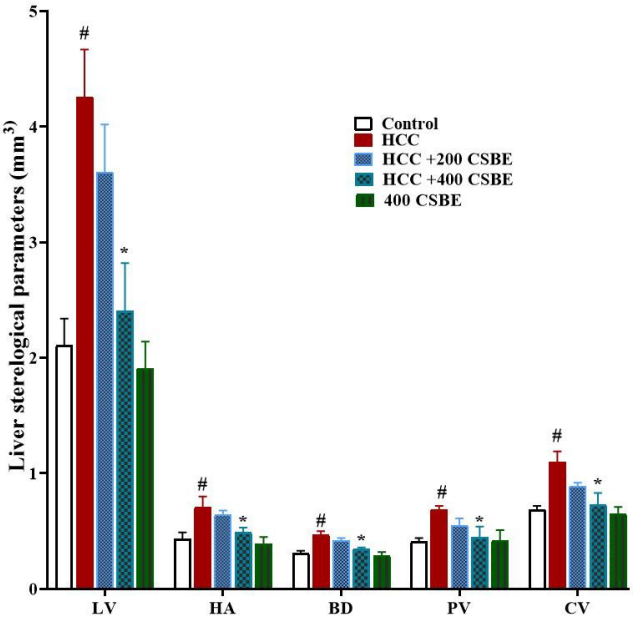

Fig. 4. Volume (mm^3) of the liver (LV), central (HA) and portal veins (PV), bile ducts (BD), and hepatic artery (HA) (mean ± standard deviation) in DEN-induced HCC in the control group and groups treated with DEN and the CSBE. # ($p<0.05$) HCC *vs.* control groups; * ($p<0.05$) HCC+200 and 400 CSBE treated *vs.* HCC groups.

Liver histopathological evaluations

Histopathological examination revealed that DEN exposure caused the formation of hepatic nodules (HN), pronounced lymphocytic infiltration (LI), and hepatocyte degeneration (D) adjacent to necrotic areas, accompanied by loss of the normal hepatic triad (HT) and hepatic lobule (HL) architecture, along with evident congestion (CO) and central venule (CV) dilatation. In contrast, the HCC + 200 and 400 CSBE groups showed restoration of normal hepatic lobule structure, marked reductions in LI, absence of HN, and clear organization of hepatocytes (H) around the liver sinusoids (S). These improvements appeared dose-dependent, with the HCC + 400 CSBE group demonstrating the most substantial recovery of tissue architecture (Fig. 5).

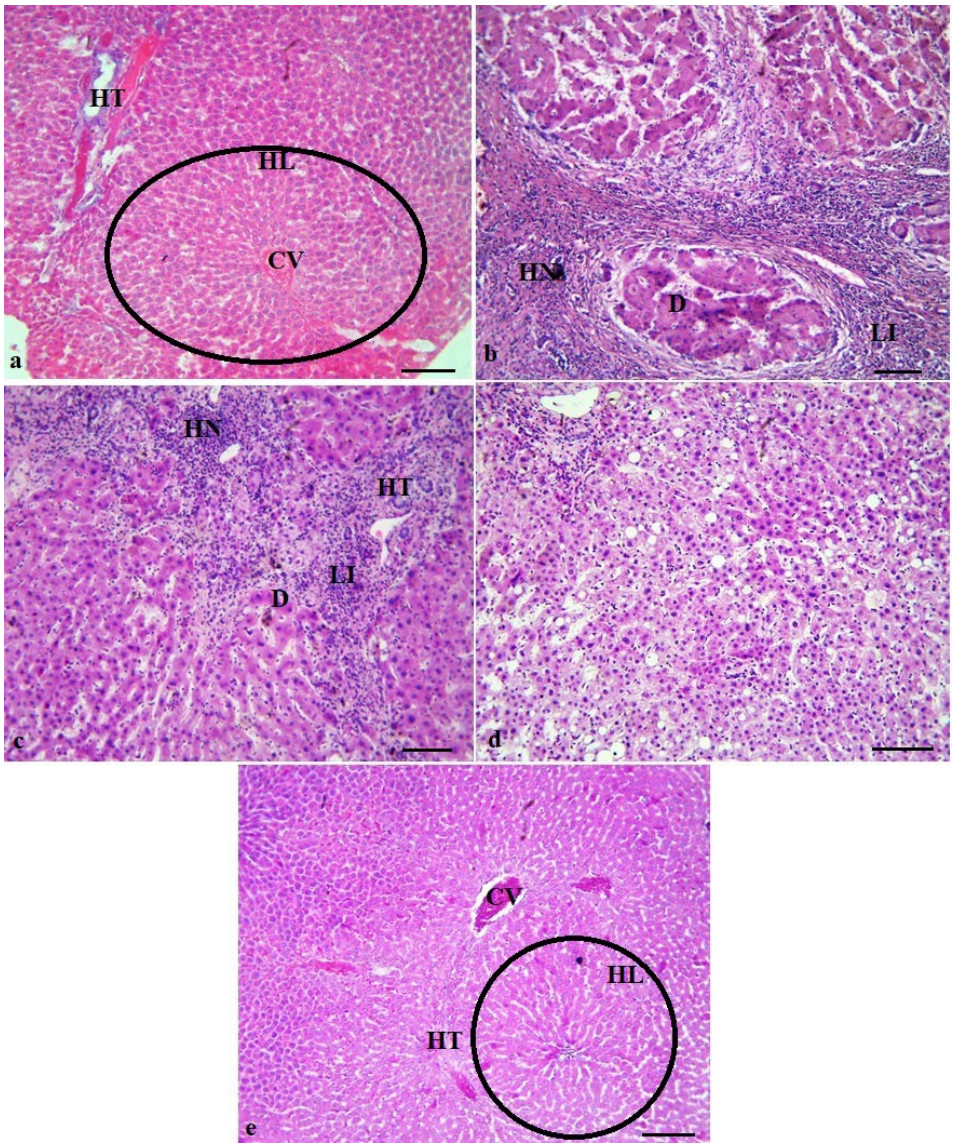

Fig. 5. Histopathological changes in liver tissue in control (a), HCC (b), HCC+200 CSBE (c), HCC+400 CSBE (d), and 400 CSBE (× 100 with Scale bar = 200 μm). Histopathological examinations of the liver tissue in the studied groups revealed that DEN induced the development of hepatic nodules (HN) consisting of lymphocytic infiltration (LI) and degenerated hepatocytes (D) near the necrotic tissue. In this specific group, the typical hepatic triad (HT) and hepatic lobule (HL) were not present, while dilatation of the central venule (CV) were visible. In the HCC+ 200 and 400 CSBE groups, the restoration of HL formation to a normal state and a significant reduction in LI were observed. Furthermore, the presence of HN was no longer identifiable in the liver, and the alignment of hepatocytes (H) alongside the liver sinusoids (S) was notably clear. These changes seem to be associated with the dosage administered, with the most significant improvement in tissue structure seen in the HCC+ 400 CSBE group.

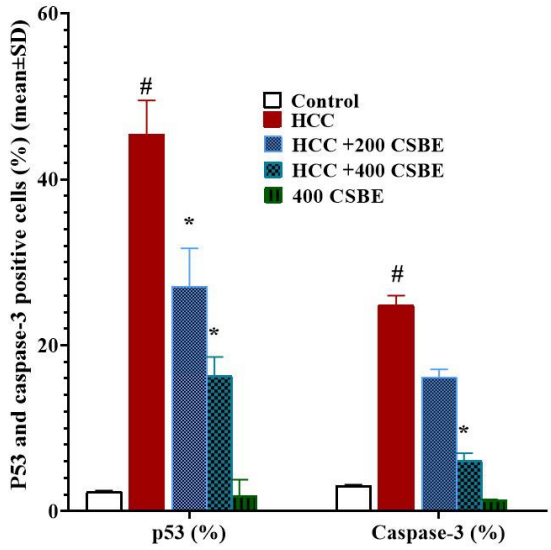

Liver p53 and caspase-3-positive hepatocytes

Analysis of p53 and caspase-3-positive cell percentages revealed that DEN administration caused a significant increase ($p < 0.05$) in p53 and caspase-3-positive cells compared with the healthy group. Treatment with CSBE extract at 200 and 400 mg/kg reduced the apoptotic index, reflected by lower p53 and caspase-3-positive cells counts relative to the HCC group. Notably, the decrease observed in the HCC + 400 CSBE group reached statistical significance compared with the HCC group (Figs. 6, 7 and 8).

Fig. 6. P53 and caspase-3 positive cells (%) in liver tissue by immunohistochemistry in experimental groups. (n=10 rat/group, data are "means ± SD). # ($p<0.05$) HCC *vs.* control groups; * ($p<0.05$) HCC+200 and 400 CSBE treated vs. HCC groups.

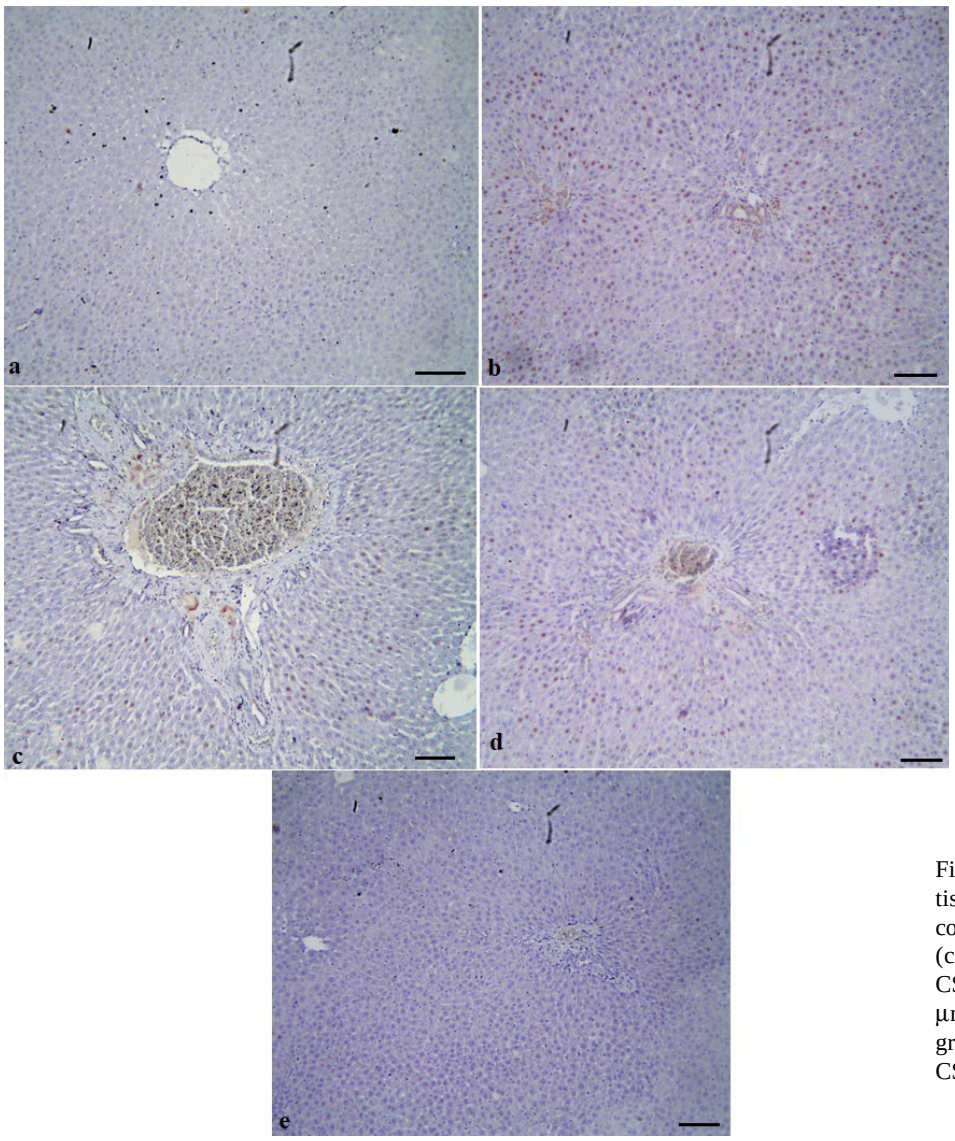

Fig. 7. P53 positive cells (%) in liver tissue by immunohistochemistry in control (a), HCC (b), HCC+200 CSBE (c), HCC+400 CSBE (d), and 400 CSBE (× 100 with Scale bar = 200 µm). # ($p<0.05$) HCC *vs*. control groups; * ($p<0.05$) HCC+200 and 400 CSBE treated *vs*. HCC groups.

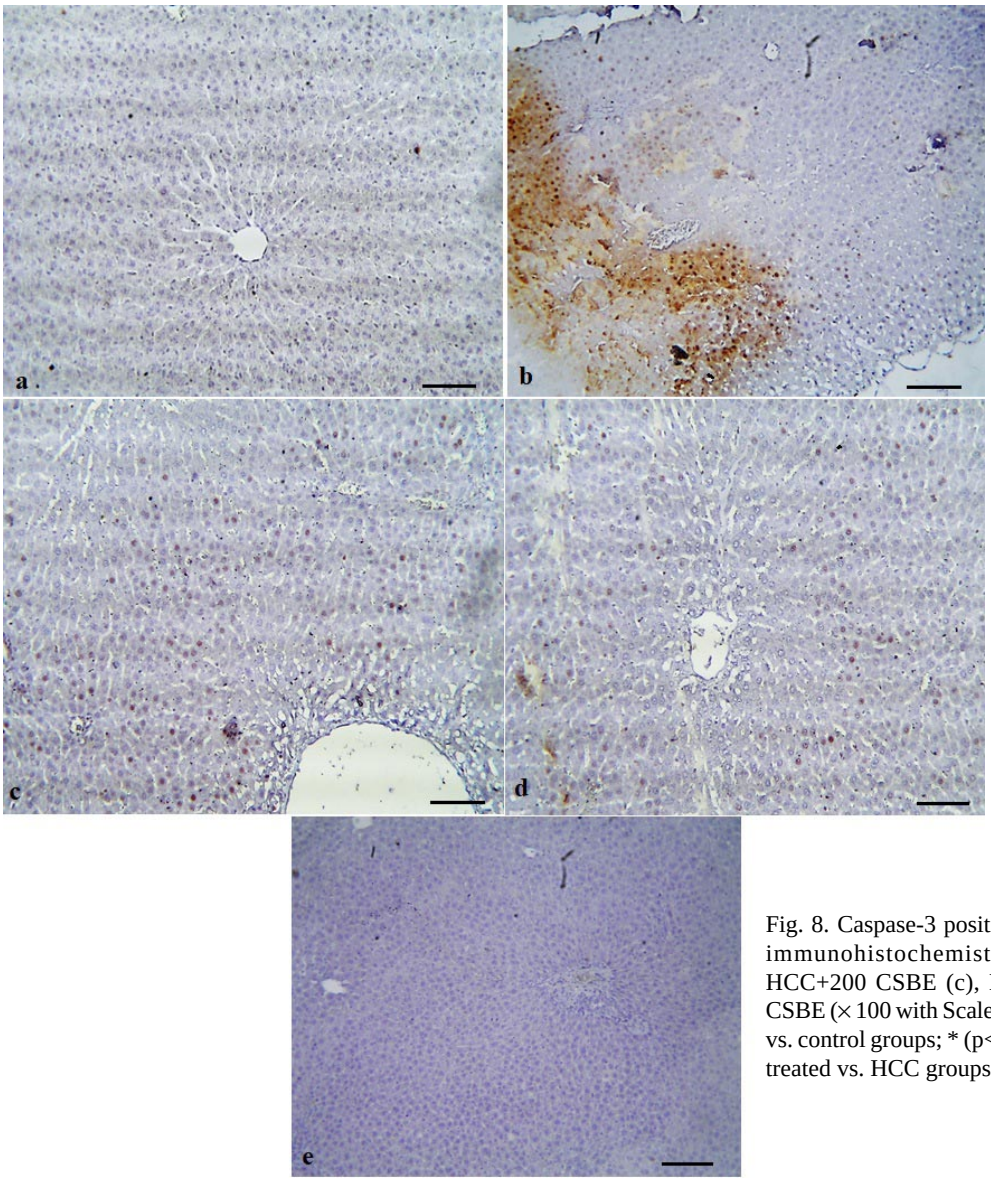

Fig. 8. Caspase-3 positive cells (%) in liver tissue by immunohistochemistry in control (a), HCC (b), HCC+200 CSBE (c), HCC+400 CSBE (d), and 400 CSBE (× 100 with Scale bar = 200 µm). # ($p<0.05$) HCC vs. control groups; * ($p<0.05$) HCC+200 and 400 CSBE treated vs. HCC groups.

DISCUSSION

Hepatocellular carcinoma remains a complex and multifactorial malignancy in which chronic inflammation, oxidative stress, dysregulated gene expression, and structural remodeling of liver tissue act synergistically to promote malignant transformation. In the present study, administration of DEN successfully reproduced the progressive biochemical and histological deterioration characteristic of human HCC, highlighting the carcinogen's well-documented hepatotoxicity. DEN's metabolic activation by cytochrome P450 enzymes yields highly reactive alkylating intermediates capable of inducing extensive DNA adduct formation, impairing genomic integrity, and activating the p53-dependent apoptotic machinery (Peng *et al*., 2024). Consistent with earlier reports by Owumi *et al*. (2019), and Alsahli *et al*. (2021), DEN exposure in our experiment markedly elevated serum ALT, AST, ALP, bilirubin, and CRP, reflecting hepatocellular leakage, disrupted bile flow, and enhanced systemic inflammation. Concurrently, total protein and albumin levels were significantly reduced, signifying impaired synthetic capacity of hepatocytes and progressive parenchymal damage. Oxidative stress emerged as a pivotal component of DEN toxicity: significant reductions in serum SOD, CAT, and GPx activities, coupled with elevated nitric oxide levels, revealed extensive free radical accumulation and compromised scavenging capacity. Tissue-level measurements reinforced this conclusion, as DEN sharply decreased thiol groups and FRAP values while increasing TBARS, indicating severe lipid peroxidation (Huang *et al*.,

2018; Singh *et al*., 2018). These biochemical alterations were mirrored at the organ level: DEN-treated rats exhibited reduced body weight, marked hepatomegaly, vascular dilation, sinusoidal distortion, bile duct attenuation, and structural collapse of hepatic lobules. Histopathological features—including hepatocyte degeneration, lymphocytic infiltration, necrotic zones, nodular formation, and architectural disarray—reflected chronic inflammatory remodeling and preneoplastic transformation. Moreover, the observed increase in p53 and caspase-3-positive hepatocytes demonstrates activation of the intrinsic apoptotic pathway, likely an early defensive response to DNA damage but simultaneously a contributor to regenerative hyperplasia and tumor-promoting cycles. At the molecular level, DEN dysregulated the HOTAIR/miR-124/Notch1 axis, a pathway increasingly recognized as a central determinant of tumor progression, stemness, and treatment resistance in HCC (Rodimova *et al*., 2023). DEN downregulated HOTAIR and Notch1 while upregulating miR-124, suggesting a profound imbalance in proliferation–apoptosis regulatory circuits. Together, these findings confirm that DEN reliably induces a multifaceted model of HCC characterized by biochemical dysfunction, massive oxidative stress, chronic inflammatory activation, genetic dysregulation, and extensive morphological deterioration, thereby providing a robust platform to evaluate the therapeutic potential of bioactive compounds such as *Ceratonia siliqua* bean extract.

The present study demonstrates that CSBE profoundly mitigates DEN-induced hepatotoxicity by restoring antioxidant equilibrium, suppressing inflammatory mediators, and improving liver function parameters in a dose-dependent manner. *Ceratonia siliqua* is rich in phenolics and flavonoids—such as catechin, gallic acid, kaempferol, and rutin—compounds known for their exceptional free radical scavenging ability, metal-chelating activity, and capacity to modulate redox-sensitive signaling pathways. The strong antioxidant effect of CSBE in our study is evidenced by the significant elevations in serum SOD, CAT, and GPx activities, reductions in nitric oxide, and restoration of hepatic thiol content, FRAP, and TBARS levels toward normal ranges. These findings indicate that CSBE attenuates oxidative challenges before they can initiate lipid peroxidation, protein oxidation, or mitochondrial dysfunction. The antioxidant response is likely mediated through upregulation of endogenous enzymatic defenses, stabilization of redox homeostasis, and scavenging of ROS/RNS generated through DEN biotransformation. Parallel to these antioxidant activities, CSBE also exerted robust anti-inflammatory effects (Hameister *et al*., 2020). DEN-induced elevations in TNF-α, IL-1β, and IL-6 were significantly reversed by CSBE, while IL-10 levels increased substantially, particularly at 400 mg/kg. Given that chronic inflammation accelerates HCC by promoting hepatocyte death, compensatory proliferation, angiogenesis, and extracellular matrix remodeling, the ability of CSBE to modulate cytokine networks is highly relevant. Its phytochemicals likely downregulate NF-κB and JAK/STAT signaling, pathways commonly activated by DEN and hyperinflammatory conditions. By reducing inflammatory stress and simultaneously enhancing anti-inflammatory counter-regulation, CSBE interrupts the feedback loops that perpetuate hepatocarcinogenesis (Ageeva *et al*., 2024). Restoration of serum ALT, AST, ALP, bilirubin, and CRP levels, along with normalization of albumin and total protein, further confirm improved hepatic integrity and synthetic function. Moreover, the significant reversal of DEN-induced body weight loss and liver enlargement indicates that CSBE not only protects hepatocytes but also prevents pathological remodeling of the liver. These collective findings align with previous studies on medicinal plants—including Vaccinium species extracts, *Trifolium pratense*, *Nigella sativa*, and *Silybum marianum*—which similarly demonstrate strong hepatic protection through antioxidant and immunomodulatory mechanisms (Abenavoli *et al*., 2018; Dalli *et al*., 2025). CSBE's multifaceted biochemical and anti-inflammatory actions thus form a central pillar of its hepatoprotective and anticancer efficacy.

Beyond its biochemical and antioxidant properties, the most striking outcome of CSBE treatment is its ability to recalibrate the HOTAIR/miR-124/Notch1 axis, a molecular network increasingly implicated in the initiation, progression, and therapeutic resistance of HCC. In DEN-injured liver tissue, downregulation of HOTAIR and Notch1, combined with upregulation of miR-124, reflects a profound shift in transcriptional regulation, epigenetic control, and cell fate determination (Feng *et al*., 2024). Dysregulation of this pathway disrupts hepatocyte differentiation cues, weakens proliferation control, and alters apoptosis–survival balance. CSBE, especially at 400 mg/kg, significantly reversed these alterations: HOTAIR, Notch1, and Jagged1 expression increased at gene levels, while miR-124 levels fell sharply toward normal values. This rebalancing suggests restoration of Notch signaling fidelity, which is essential for hepatic homeostasis, lineage maintenance, and controlled regeneration. Contrary to classical views of Notch as exclusively oncogenic, its role in liver biology is context-dependent: early carcinogenesis requires Notch suppression to enable uncontrolled dedifferentiation, while restored Notch activity can promote hepatocyte maturation and restrain malignant transformation (Valizadeh *et al*., 2021). By upregulating Notch1 and Jagged1, CSBE may reinforce controlled proliferation and prevent aberrant dedifferentiation—a hallmark of DEN-induced carcinogenesis. Additionally, the modulation of HOTAIR, a

long non-coding RNA involved in chromatin remodeling, suggests epigenetic reprogramming. The normalization of HOTAIR expression indicates that CSBE may prevent histone modification patterns that promote invasive and metastatic phenotypes (Mozdarani *et al*., 2020). The downregulation of miR-124, a microRNA known to suppress Notch signaling, further reinforces pathway restoration. Importantly, CSBE also reduced p53 and caspase-3-positive apoptotic hepatocytes, suggesting mitigation of DNA damage and prevention of excessive apoptotic turnover—a key factor in limiting compensatory proliferation and reducing carcinogenic pressure. Histological improvements, including restored lobular architecture, reduced lymphocytic infiltration, absence of hepatic nodules, and normalized vascular and bile duct volumes, corroborate the molecular findings. These tissue-level outcomes highlight CSBE's capacity to attenuate the destructive cycle of inflammation-driven apoptosis, regeneration, and neoplastic transformation. The concurrent regulation of oxidative stress pathways, inflammatory cytokines, and the HOTAIR/miR-124/Notch1 axis underscores a comprehensive therapeutic profile, positioning CSBE alongside other plant-derived bioactives—such as curcumin, resveratrol, quercetin, and Vaccinium polyphenols—which similarly modulate oncogenic and tumor-suppressive signaling networks in HCC (Batiha *et al*., 2020). Importantly, CSBE's efficacy was dose-dependent, with the 400 mg/kg dosage consistently outperforming the 200 mg/kg treatment across all biochemical, molecular, and histological metrics, suggesting a threshold concentration required for optimal modulation of the DEN-induced pathological cascade. Additionally, the LD50 value of 3162 mg/kg confirms a high safety margin, supporting further pharmacological development. The implications of these findings extend beyond preclinical modeling: by demonstrating the capacity of CSBE to regulate lncRNA–microRNA–Notch signaling, our results identify actionable molecular targets for future therapeutic exploitation. This is particularly relevant given that dysregulation of HOTAIR, miR-124, and Notch1 correlates with poor prognosis, metastasis, and chemoresistance in human HCC. Thus, CSBE may serve as a foundation for novel combination therapies, potentially enhancing the efficacy of existing treatments such as sorafenib or immunomodulatory agents.

CONCLUSION

This study demonstrates that CSBE provides significant hepatoprotective and anticancer effects against DEN-induced hepatocellular carcinoma through coordinated biochemical, molecular, and histopathological mechanisms. CSBE effectively restored liver function markers, enhanced antioxidant defenses, reduced inflammatory cytokines, and normalized oxidative stress parameters. Its modulation of the HOTAIR/miR-124/Notch1 signaling axis, along with the reduction in p53 and caspase-3-positive apoptotic cells, highlights its capacity to regulate key pathways involved in hepatocyte proliferation, differentiation, and survival. Histopathological improvements—including restored lobular structure, reduced lymphocytic infiltration, and absence of hepatic nodules—further support its protective role. Notably, the 400 mg/kg dose exhibited the most pronounced therapeutic benefits, indicating a dose-dependent response. Overall, these findings suggest that CSBE is a promising natural agent for preventing or attenuating hepatocarcinogenesis and warrants further investigation as a complementary strategy in liver cancer management.

Funding. Establishment and Development of a Database and Biobank for Populations at High Risk of Hepatocellular Carcinoma in Yongkang City (No. 202407002).

Conflicts of interest.The author(s) declared no potential conflicts of interest with respect to the research, authorship, and/or publication of this article.

Ethical statement. This research adhered to ethical guidelines for the use of animal subjects. Animal welfare considerations were taken into account, minimizing pain, distress, and suffering. Ethical approval was obtained from the Institutional Animal Care and Use Committee of Zhejiang Ailimo Biotechnology Co., Ltd (ALM20251130).

GAO, X.; YING, X.; CHEN, D.; CHEN, Z.; LV, X. & WANG, J. Investigación de los efectos anticancerígenos del extracto de algarrobo *Ceratonia siliqua* L. sobre el carcinoma hepatocelular: perspectivas sobre las vías inflamatorias, del estrés oxidativo y HOTAIR/miR-124/Notch1 mediante métodos bioquímicos, moleculares, inmunohistoquímicos e histopatológicos. *Int. J. Morphol., 44(3)*:789-802, 2026.

RESUMEN: Este estudio evaluó el potencial hepatoprotector y anticancerígeno del extracto de algarrobo (CSBE) de *Ceratonia siliqua* L. (algarrobo) frente al carcinoma hepatocelular (CHC) inducido por N-dietilnitrosamina (DEN) en ratas Wistar, centrándose en su modulación de vías bioquímicas, antioxidantes y moleculares, incluyendo el eje HOTAIR/miR-124/Notch1. Cincuenta ratas se dividieron en cinco grupos: controles normales, CHC inducido por DEN (80 mg/kg), CHC tratado con 200 o 400 mg/kg de CSBE, y ratas normales que recibieron 400 mg/kg de CSBE. Las evaluaciones posteriores al tratamiento incluyeron marcadores séricos de la función hepática (albúmina, proteína total, bilirrubina, PCR, ALT, AST, ALP), citocinas inflamatorias (IL-6, IL-1β, IL-10, TNF-α), parámetros de estrés oxidativo (GPx, SOD, CAT, óxido nítrico) y análisis molecular de la expresión de HOTAIR, miR-124, Notch1 y Jagged1 en tejido hepático, junto con inmunotinción de p53 y caspasa-3. La administración de DEN alteró el peso

corporal y hepático, elevó las enzimas hepáticas, deterioró las defensas antioxidantes y desreguló el eje HOTAIR/miR-124/Notch1, mientras que CSBE, particularmente a 400 mg/kg, restauró la función hepática de forma dosis-dependiente, redujo el estrés oxidativo y la inflamación, normalizó la expresión génica y mejoró la arquitectura histopatológica. Estos hallazgos demuestran la eficacia de CSBE para mitigar el CHC inducido por DEN a través de mecanismos multifacéticos, lo que resalta su potencial terapéutico.

PALABRAS CLAVE: *Ceratonia siliqua* L.; N-dietilnitrosamina; HOTAIR; Hígado; Carcinoma hepatocelular.

REFERENCES

Abenavoli, L.; Izzo, A. A.; Milic, N.; Cicala, C.; Santini, A. & Capasso, R. Milk thistle (*Silybum marianum*): a concise overview on its chemistry, pharmacological, and nutraceutical uses in liver diseases. *Phytother. Res., 32(11)*:2202-13, 2018.

Ageeva, T.; Rizvanov, A. & Mukhamedshina, Y. NF-kB and JAK/STAT signaling pathways as crucial regulators of neuroinflammation and astrocyte modulation in spinal cord injury. *Cells, 13(7)*:581, 2024.

Alsahli, M. A.; Almatroodi, S. A.; Almatroudi, A.; Khan, A. A.; Anwar, S.; Almutary, A. G. & Rahmani, A. H. 6-Gingerol, a major ingredient of ginger attenuates diethylnitrosamine-induced liver injury in rats through the modulation of oxidative stress and anti-inflammatory activity. *Mediators Inflamm., 2021*:6661937, 2021.

Aydemir, D. & Ulusu, N. N. *The Impact of Rosmarinic Acid on the Oxidative Stress Metabolism: Evaluation Protocol Based on Glutathione-Dependent and -Independent Antioxidant Enzymes*. In: Gouda, M.; Li, X. & He, Y. (Eds.). Plant Chemical Compositions and Bioactivities. Methods and Protocols in Food Science. New York, Humana, 2024.

Batiha, G. E. S.; Beshbishy, A. M.; Ikram, M.; Mulla, Z. S.; El-Hack, M. E. A.; Taha, A. E. & Elewa, Y. H. A. The pharmacological activity, biochemical properties, and pharmacokinetics of the major natural polyphenolic flavonoid: quercetin. *Foods, 9(3)*:374, 2020.

Dahmani, W.; Elaouni, N.; Abousalim, A.; Akissi, Z. L. E.; Legssyer, A.; Ziyyat, A. & Sahpaz, S. Exploring carob (*Ceratonia siliqua* L.): a comprehensive assessment of its characteristics, ethnomedicinal uses, phyto*chemical aspects, and pharmacological activities*. Plants (Basel), 12(18):3303, 2023.

Dalli, M.; Daoudi, N. E.; Azizi, S. E.; Roubi, M.; Alami Merrouni, I.; Souna, F.; Choukri, M.; Kim, B. & Gseyra, N. Harnessing the hepatoprotective and nephroprotective potential of *Nigella sativa* fractions via per os administration in CCl4-intoxicated Wistar rats: a mixed approach. *Pharmaceuticals (Basel), 18(8)*:1147, 2025.

El Sayed, N. S.; Abidar, S.; Nhiri, M.; Hritcu, L. & Ibrahim, W. W. Aqueous extract of *Ceratonia siliqua* L. leaves elicits antioxidant, anti-inflammatory, and AChE inhibiting effects in amyloid-b42-induced cognitive deficit mice: role of a7-nAChR in modulating Jak2/PI3K/Akt/GSK-3b/b-catenin cascade. *Phytother. Res., 37*:2437-53, 2023.

Feng, H.; Zheng, S.; Yang, J.; Mao, X.; Liu, T.; Zhang, Q. & Chen, Y. Exploring the anti-cancer properties of Nasturtium officinale L. via the HOTAIR/miR-124/Notch1 pathway in rat hepatocellular carcinoma: An investigation using biochemical, molecular, immunohistochemical, and histopathological methods. *Int. J. Morphol., 42(5)*:1361-72, 2024.

Hameister, R.; Kaur, C.; Dheen, S. T.; Lohmann, C. H. & Singh, G. Reactive oxygen/nitrogen species (ROS/RNS) and oxidative stress in arthroplasty. *J. Biomed. Mater. Res. B Appl. Biomater., 108(5)*:2073-87, 2020.

Huang, D.; Li, H.; He, Q.; Yuan, W.; Chen, Z. & Yang, H. Developmental toxicity of diethylnitrosamine in zebrafish embryos/juveniles related to excessive oxidative stress. *Water Air Soil Pollut., 229(3)*:81, 2018.

Janmeda, P.; Jain, D.; Chaudhary, P.; Meena, M. & Singh, D. A systematic review on multipotent carcinogenic agent, N-nitrosodiethylamine (NDEA), its major risk assessment, and precautions. *J. Appl. Toxicol., 44(8)*:1108-28, 2024.

Karimian, M.; Ghadiri, M.; Poormoosavi, S. M. & Najafzadehvarzi, H. Protective effects of resveratrol on the expression of catalase, glutathione peroxidase, and superoxide dismutase genes in the ovary and their activity in the serum of rats exposed to lead acetate: an experimental study. *Int. J. Reprod. Biomed., 22(11)*:883-94, 2025.

Khorshed, F.; Medhat, A. M.; Hamdy, G. M.; El-Dabaa, E.; Hammad, H.; Elhameed, H. A. A. & Saber, M. Novel perspective of regulating p53/Bcl2/Caspase-3 via in vitro targeted AFP gene knocks out in HepG2 cells using CRISPR/Cas9 editing tool. *Curr. Gene Ther., 2025*. Doi: 10.2174/0115665232366303250529164610

Kotsari, M.; Dimopoulou, V.; Koskinas, J. & Armakolas, A. Immune system and hepatocellular carcinoma (HCC): new insights into HCC progression. *Int. J. Mol. Sci., 24(14)*:11471, 2023.

Li, Y.; Liu, Y.; Wang, S. & Li, W. Exploring the anti-seborrheic dermatitis effects of apricot kernel oil using the rat-dinitrofluorobenzene induced model: an investigation using biochemical, molecular, and histopathological methods. *Int. J. Morphol., 43(2)*:564-73, 2025.

Ma, B. & Wang, R. Therapeutic potential of hydroalcoholic extract of Rumex alveollatus L. leaves in atherosclerosis: biochemical, molecular, and histopathological insights from a rat model. *Pharmacogn. Mag., 22(2)*:09731296251350747, 2025.

Ma, H. Y.; Dong, L.; Quan, S. Z.; Li, R. Y. & Wang, X. R. Comparison of four markers of hepatic fibrosis and hepatic function indices in patients with liver cirrhosis and hepatoma. *Ann. Palliat. Med., 10(4)*:4108-21, 2021.

Mi, G.; Li, B.; Gong, X.; Wu, J.; Zhang, Y.; Ma, L. & Sheng, L. Human adipose-derived stem cells promote axonal growth and survival of rat retinal ganglionic cells through anti-inflammatory, anti-oxidant, anti-apoptotic, and paracrine stimulation via the PI3K/Akt pathway. *Int. J. Morphol., 42(6)*:1464-73, 2024.

Mozdarani, H.; Ezzatizadeh, V. & Rahbar Parvaneh, R. The emerging role of the long non-coding RNA HOTAIR in breast cancer development and treatment. *J. Transl. Med., 18(1)*:152, 2020.

Naseri, L.; Khazaei, M.; Ghanbari, E. & Bazm, M. A. Rumex alveollatus hydroalcoholic extract protects CCL4-induced hepatotoxicity in mice. *Comp. Clin. Pathol., 28*:557-65, 2019.

Owumi, S. E.; Dim, U. J. & Najophe, E. S. Diethylnitrosamine aggravates cadmium-induced hepatorenal oxidative damage in prepubertal rats. *Toxicol. Ind. Health, 35(8)*:537-47, 2019.

Peng, C.; Ye, Z.; Na, J.; Liu, X. & Zhang, Z. Establishment and refinement of a DEN-induced hepatocellular carcinoma model in rats. *Oncologie, 26(3)*:419-31, 2024.

Rodimova, S.; Mozherov, A.; Elagin, V.; Karabut, M.; Shchechkin, I.; Kozlov, D.; Krylov, D.; Gavrina, A.; Bobrov, N.; Zagainov, V.; *et al*. Effect of hepatic pathology on liver regeneration: the main metabolic mechanisms causing impaired hepatic regeneration. *Int. J. Mol. Sci., 24(11)*:9112, 2023.

Singh, D.; Singh, M.; Yadav, E.; Falls, N.; Komal, U.; Dangi, D. S. & Verma, A. Amelioration of diethylnitrosamine (DEN)-induced hepatocellular carcinogenesis in animal models via knockdown oxidative stress and proinflammatory markers by Madhuca longifolia embedded silver nanoparticles. *RSC Adv., 8(13)*:6940-53, 2018.

Tabakhiyan, F.; Mir, A. & Vahedian, V. Potential tumor marker for hepatocellular carcinoma identification: PI3K and pro-inflammatory cytokines (TGF-β, IL-1, and IL-6). *Horm. Mol. Biol. Clin. Investig., 43(4)*:389-96, 2022.

Thomas, P. A.; García-Martí, X.; Mukassabi, T. A. & Tous, J. International Biological Flora: *Ceratonia siliqua*: No. 4. *J. Ecol., 112*:1885-922, 2024.

Valizadeh, A.; Sayadmanesh, A.; Asemi, Z.; Alemi, F.; Mahmoodpoor, A. & Yousefi, B. Regulatory roles of the Notch signaling pathway in liver repair and regeneration: a novel therapeutic target. *Curr. Med. Chem., 28(41)*:8608-26, 2021.

Wang, Y. K.; Tydlitatova, L.; Kunz, J. D.; Oakley, G.; Chow, B. K. B.; Godrich, R. A.; Lee, M. C. H.; Aghdam, H.; Bozkurt, A.; Zelechowski, M.; *et al*. Screen them all: high-throughput pan-cancer genetic and phenotypic biomarker screening from H&E whole slide images. *arXiv:*2408.09554, 2024.

Wang, Z.; Jiang, X.; Zhang, L. & Chen, H. Protective effects of Althaea officinalis L. extract against N-diethylnitrosamine-induced hepatocellular carcinoma in male Wistar rats through antioxidative, anti-inflammatory, mitochondrial apoptosis and PI3K/Akt/mTOR signaling pathways. *Food Sci. Nutr., 11(8)*:4756-72, 2023.

Yu, J.; Zhu, C.; Wang, X.; Kim, K.; Bartolome, A.; Dongiovanni, P.; Yates, K. P.; Valenti, L.; Carrer, M.; Sadowski, T.; *et al*. Hepatocyte TLR4 triggers inter-hepatocyte Jagged1/Notch signaling to determine NASH-induced fibrosis. *Sci. Transl. Med., 13(599)*:eabe1692, 2021.

Zhang, J.; Li, N.; Lu, S.; Chen, Y.; Shan, L.; Zhao, X. & Xu, Y. The role of Notch ligand Jagged1 in osteosarcoma proliferation, metastasis, and recurrence. *J. Orthop. Surg. Res., 16*:226, 2021.

Zhou, C.; Qin, X.; Wang, J. & Liu, Y. Anticancer effects of Vaccinium arctostaphylos L. through HOTAIR/miR-124/Notch1 axis of hepatocellular carcinoma in rat: a biochemical, molecular, immunohistochemical, and histopathological approaches. *Pharmacogn. Mag., 20(4)*:1114-27, 2024.

Corresponding author:
Junbao Wang
Department of General Surgery
The First People's Hospital of Yongkang (Yongkang First People's Hospital)
No. 599 Jinshan West Road
Yongkang City
Jinhua
Zhejiang Province 321300
CHINA

E-mail: gxb94666@outlook.com
wjb2583692023@163.com